

1 Two-dimensional monitoring of air pollution in Madrid using a
2 MAXDOAS-2D instrument

3

4 David Garcia-Nieto^{1, 2}, Nuria Benavent^{1, 2}, Rafael Borge² and Alfonso
5 Saiz-Lopez¹

6

7 ¹ Department of Atmospheric Chemistry and Climate, Institute of
8 Physical Chemistry Rocasolano, CSIC, Madrid 28006, Spain

9 ² Universidad Politécnica de Madrid, UPM, 28006 Madrid, Spain

10

11 *Corresponding author: Alfonso Saiz-Lopez (a.saiz@csic.es)

12

13 Abstract

14

15 Trace gases play a key role in the chemistry of urban atmospheres.
16 Therefore, knowledge about their spatial distribution is needed to
17 fully characterize the air quality in urban areas. Using a new Multi-
18 AXis Differential Optical Absorption Spectroscopy (MAXDOAS)-2D
19 instrument, along with an inversion algorithm (bePRO), we report the
20 first two-dimensional maps of nitrogen dioxide (NO₂) and nitrous acid
21 (HONO) concentrations in the city of Madrid, Spain. Measurements were
22 made during two months (May 6 -July 5 2019) and peak mixing ratios of
23 12 ppbv and 0.7 ppbv for NO₂ and HONO, respectively, were observed in
24 the early morning in the south-pointing geometry. We found good general
25 agreement between the MAXDOAS-2D mesoscale observations -which provide
26 a typical spatial range of a few kilometers- and the in-situ
27 measurements provided by Madrid's air quality monitoring stations. In
28 addition to vertical profiles, we studied the horizontal gradients of
29 NO₂ in the surface layer by applying the different horizontal light
30 path lengths in the two spectral regions included in the NO₂ spectral

31 analysis: ultraviolet (UV, at 360 nm) and visible (VIS, 477 nm). We
32 also investigate the sensitivity of the instrument to infer vertically-
33 distributed information on aerosol extinction coefficients and discuss
34 possible future ways to improve the retrievals. The retrieval of two-
35 dimensional distributions of trace gas concentrations reported here
36 provides valuable spatial information for the study of air quality in
37 the city of Madrid.

38

39 1 Introduction

40

41 Air pollution in urban areas has become a concern in our society
42 because it represents a major risk to human health and the environment
43 (WHO, 2019). Air quality is often expressed as the state of air
44 pollution in terms of gaseous pollutant concentrations as well as size
45 and number of particulate matter that may affect human health,
46 ecosystems and climate (Monks et al., 2009). Integral understanding
47 of air pollution requires knowledge about the sources, pollutants,
48 chemical composition and spatial distribution, and their transport
49 phenomena in the atmosphere (EEA, 2019).

50

51 Madrid, Spain, has suffered from severe air pollution in recent
52 years, with episodes of large nitrogen dioxide (NO₂) and ozone (O₃)
53 concentrations. In an effort to control and reduce high pollution
54 events, the local government has enforced some traffic restriction
55 measures (Izquierdo et al., 2020) and has set up several in-situ air
56 quality monitoring stations over the city's metropolitan area. These
57 in-situ instruments -as of today- cannot measure some important trace
58 gases present in the atmosphere and their values are only
59 representative of the immediate surrounding of the instruments and at
60 surface level. There is therefore a need for mesoscale analysis (both
61 in horizontal and vertical) of urban air pollution that could
62 complement the in-situ measurements. With this aim, we have deployed

63 a Multi AXis Differential Optical Absorption Spectroscopy (MAXDOAS)
64 instrument for air pollution measurements in Madrid. MAXDOAS is a
65 widely used technique for the detection of trace gases in the
66 atmosphere and it is based on the wavelength dependent absorption of
67 scattered sunlight by atmospheric constituents (Platt and Stutz,
68 2008). In addition to routinely monitored, regulated species such as
69 NO₂ and O₃, MAXDOAS provides mesoscale measurements of other trace
70 gases that are relevant to understand atmospheric chemistry, such as
71 nitrous acid (HONO), formaldehyde (HCHO) or glyoxal (CHOCHO). Over the
72 past few years, we have reported trace gas measurements in Madrid
73 using the MAXDOAS technique (Wang et al., 2016; Garcia-Nieto et al.,
74 2018; Benavent et al., 2019) as well as pollutants trend analysis and
75 chemical transport modelling (Borge et al., 2018; Cuevas et al., 2014;
76 Saiz-Lopez et al., 2017).

77

78 For this work, a new two-dimensional MAXDOAS instrument (which
79 will be described in Sect. 3 and will be hereafter referred to as
80 MAXDOAS-2D) has been built, tested and set up to take continuous
81 measurements in Madrid. This instrument represents a follow-up
82 development to our previous one-dimensional instrument (MAXDOAS-1D,
83 see Wang et al., 2016) that incorporates the capability of moving in
84 the azimuthal dimension, therefore allowing the collection of spectra
85 pointing at any angular direction. This additional capability allows
86 the measurement of both the horizontal and vertical trace gas (e.g.
87 NO₂) distribution throughout the city and in turn the generation of
88 two-dimensional maps of trace gas concentrations. Several works using
89 two-dimensional MAXDOAS instruments have been carried out in recent
90 years (e.g. Ortega et al., 2015, Yang et al., 2019, Schreier et al.,
91 2019, Dimitropolou et al., 2020). These studies were mostly focused
92 on mapping the NO₂ distribution in urban environments and assessing
93 its role for air quality monitoring.

94

95 Here we present two months of MAXDOAS-2D measurements of
96 scattered sunlight spectra. The measurements were taken from May 6,
97 2019 to July 5, 2019, with focus on the evaluation of NO₂ vertical
98 concentration profiles and the characterization of horizontal light
99 path lengths. We will also provide the retrieval of HONO as an example
100 of the potential of the MAXDOAS-2D measurements. This represents the
101 first two-dimensional MAXDOAS measurements in Madrid. An assessment
102 of the relation between the MAXDOAS analysis and the in-situ
103 instruments in the city was carried out. Sect. 2 provides details of
104 the DOAS technique while Sect. 3 describes the experimental setup. The
105 inversion methods and the atmospheric parameters chosen for the
106 analysis is detailed in Sect. 4. The two-dimensional NO₂ and HONO
107 distributions, an evaluation of the light path geometries, along with
108 their relative probabilities, and an assessment of horizontal mixing
109 ratio gradients near the surface are discussed in Sect. 5. Finally,
110 Sect. 6 contains conclusions and possible future work.

111

112 2 Brief introduction to the DOAS method

113

114 The absorption spectroscopy field has been developed for several
115 decades within different research disciplines (such as remote sensing,
116 astronomy or atomic and molecular physics). Its foundation relies on
117 the absorption of radiation when interacting with a certain sample.
118 The basic idea is described by the Beer-Lambert law, which models the
119 exponential attenuation of spectral irradiance when it traverses a
120 certain sample that contains some absorber species:

121

$$122 \quad I(\lambda, L) = I_0(\lambda) \exp \left(- \sum_i \int_0^L \sigma_i(\lambda) \rho_i(s) ds \right) \quad (1)$$

123

124 where λ is the radiation wavelength, σ_i and ρ_i stand for -
125 respectively- the absorption cross section and concentration of
126 a given absorber i along the path, while the pair I_0 and I
127 represent the spectral irradiances at the beginning and end of
128 the process at study. The absorption processes are integrated
129 over the photon paths (with infinitesimal path ds) and summed
130 over every present absorber (Platt and Stutz, 2008).

131

132 Specifically, the MAXDOAS technique is based on the study of the
133 differential spectral absorption structures that are produced in the
134 measured scattered sunlight spectra (Hönninger et al., 2004; Plane and
135 Saiz-Lopez, 2006; Platt and Stutz, 2008). The main principle is based
136 on identifying the narrowband absorption features within the measured
137 optical density taking out the broadband optical density, mainly
138 generated by Rayleigh and Mie scattering, as well as by instrumental
139 effects. On the other hand, an analogous process is done on the trace
140 gases absorption cross sections by means of filtering out the broadband
141 spectral features, hence producing the so-called differential
142 absorption cross sections, which are unique for each trace gas, acting
143 as their “fingerprints” and therefore enabling their specific
144 detection.

145

146 For MAXDOAS, I_0 stands for the solar spectrum (known as the
147 Fraunhofer spectrum, with no Earth atmospheric absorptions), while I
148 represents the recorded ground-based spectrum, which includes all the
149 absorption and scattering processes. However, and since the actual
150 photon path is difficult to determine with accuracy (see Sect. 4), the
151 MAXDOAS calculations are done using relative absorptions between two
152 different optical paths: a zenith spectrum -that contains less
153 absorptions and is assumed as a reference spectrum- and other spectrum
154 pointing to a given elevation angle. Therefore, the direct product of
155 the method is the Differential Slant Column Density (DSCD), which can

156 be defined as the difference in the integrated concentration of a
157 given absorber between the two selected pointing directions (more
158 details about the numerical procedure that lies behind can be found
159 in Honninger et al., 2004, Plane and Saiz-Lopez, 2006 and Platt and
160 Stutz, 2008). Finally, these DSCDs are used as the main input for the
161 profile retrieval algorithms, which simulate the state of the
162 atmosphere with the purpose of reproducing the measured DSCDs. This
163 final step yields the optimal vertical concentration profiles.

164

165 3 Experimental

166

167 Briefly, MAXDOAS-1D instruments consist of a light collector
168 attached to a stepper motor that scans the atmosphere at different
169 Viewing Elevation Angles (VEA, see Fig. 1). The main feature added to
170 the MAXDOAS-2D instrument is an additional stepper motor for the
171 azimuthal movement, hence allowing the light collector to freely point
172 to any angular direction in the atmosphere. This allows the evaluation
173 of trace gases absorptions for different Viewing Azimuth Angles (VAAs)
174 (Fig. 1).

175

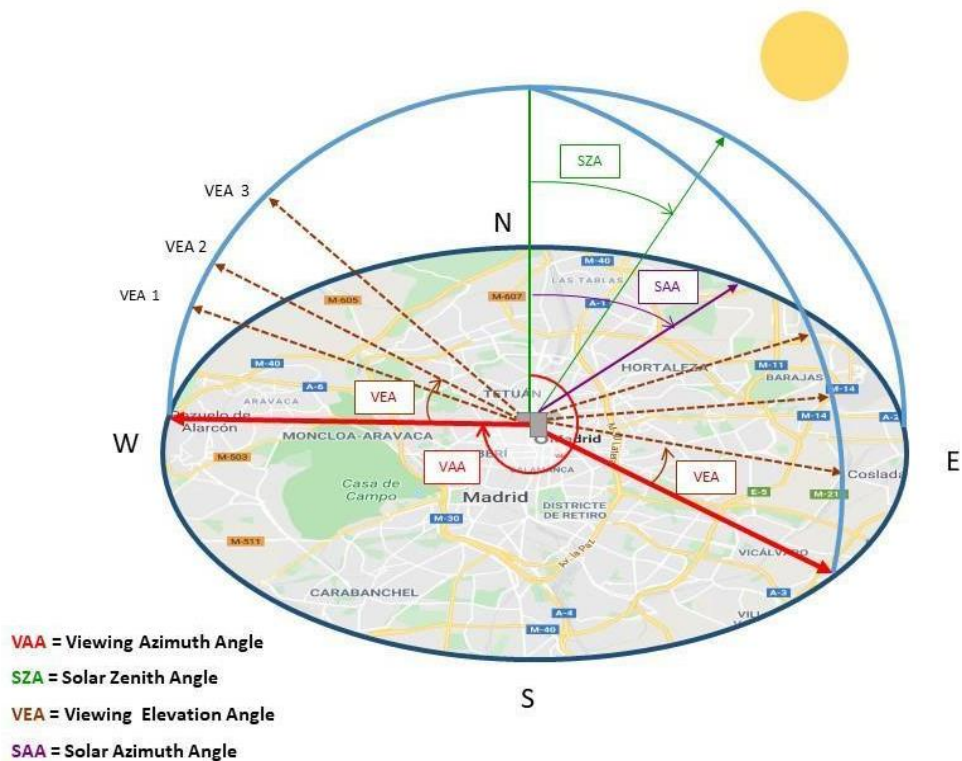
176 3.1 MAXDOAS-2D description

177

178 A new MAXDOAS-2D instrument (Fig. 2) was built by the Atmospheric
179 Chemistry and Climate group at the Institute of Physical Chemistry
180 Rocasolano (IQFRCSIC). Its main elements are based on our previous
181 MAXDOAS-1D instrument: a light collector attached to a stepper motor,
182 along with a focusing lens (80 mm focal length) are responsible for
183 collecting the scattered sunlight. An Ocean Optics, SMA 905 optical
184 fiber of 1-meter length conducts the light through an Ocean Optics,
185 HR4000 spectrometer (which incorporates a linear silicon CCD array as
186 detector). The spectrometer wavelength ranges roughly from 300 nm to

187 500 nm and offers an estimated spectral resolution (full width at half
 188 maximum) of about 0.5 nm. An additional stepper motor was included for
 189 azimuthal movement. The instrument incorporates all its components in
 190 an outdoor unit. Therefore, to maintain the spectrometer temperature
 191 as steady as possible -for both mechanical and wavelength calibration
 192 purposes- a Peltier cell was included. Additionally, an UPS device
 193 provides the power supply and eliminates possible strong power peaks.
 194 Two webcams take pictures of the cloud cover at each VAA, and monitor
 195 the instrument itself. The instrument is autonomous and it runs on a
 196 homemade Java software. This software controls the movement, the
 197 spectra collection and recording, the surrounding accessories and
 198 automatically keeps it continuously measuring as long as the Sun is
 199 over the horizon.

200



201

202 Figure 1. MAXDOAS-2D geometry diagram, the background of this
 203 picture represents the Madrid city center taken from Google Maps.

204

205 3.2 Location

206

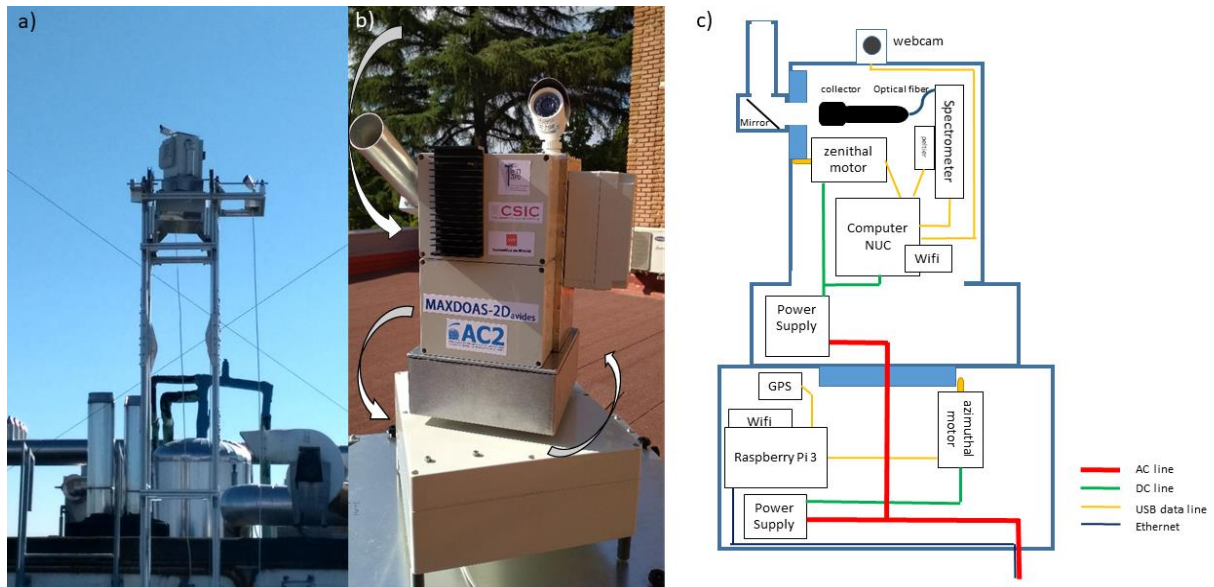
207 The MAXDOAS-2D instrument is located at the main campus of the
208 Spanish National Research Council (CSIC) in Madrid, Spain. It is placed
209 on the roof of the Instituto de Ciencias Agrarias (ICA) at a latitude
210 of 40.4419° N and a longitude of 3.6875° W. The height of the building
211 is approximately 70 m above ground level. This location in downtown
212 Madrid can be classified as an urban site, with the usual weather of
213 continental areas at mid-latitudes (i.e. hot and dry summers and cold
214 winters), with prevalence of clear sky days during the year. NO_2
215 typically presents strong spatial concentration gradients in urban
216 areas and traffic hot-spots have been reported in Madrid (Borge et
217 al., 2016). This makes it difficult to clearly predict how NO_2 will be
218 distributed, i.e., there is not a clear azimuthal direction preference
219 for higher NO_2 at a certain time. However, mesoscale simulations
220 suggest that higher NO_2 mixing ratios can be expected in the southern
221 part of Madrid, considering population distribution and commuting
222 patterns (Picornell et al., 2019).

223

224 Due to some obstacles that blocked a clear view in some of the
225 VAAs, a small aluminum tower was built to overcome the viewing
226 obstacles and the MAXDOAS-2D instrument was fixed on top of it (see
227 Fig. 2). Once the instrument was set up, we aligned it for both angular
228 movements -azimuthal and zenithal- with respect to the geographical
229 north and the local horizontal (i.e. perpendicular to the gravitational
230 plumb), respectively. This process was performed in two steps: first,
231 the light collector was coarsely oriented using levels and a compass.
232 Then, the alignment was refined doing a vertical scan of the Sun (which
233 has a very well-known position vector) and its angular surroundings
234 at several different times of a clear sky day. The angular differences
235 between the measurements and the center of intensity of the registered

236 spectra (a similar approach was done in Ortega et al., 2015) were
237 estimated and the associated correction applied to the instrument.

238



239

240 Figure 2. a) Aluminum tower with the instrument installed on top of
241 it; b) MAXDOAS-2D instrument; c) MAXDOAS-2D scheme.

242

243 3.3 Measurements set up

244

245 In order to sample and analyze a representative portion of the
246 atmosphere over Madrid, selected angular directions were chosen.
247 Starting at a VAA of 0° (pointing to the north), the MAXDOAS-2D rotated
248 clockwise using steps of 20° in azimuth. In each azimuth direction,
249 the ensuing VEA vector was used: 1, 2, 3, 5, 10, 30 and 90 degrees.
250 Therefore, an entire azimuthal lap was completed when the light
251 collector was back again at VAA of 0 degrees.

252

253 For every measured spectrum, the spectrometer was able to correct
254 for both electronic offset and dark current effects. Other important
255 parameters for the measurements such as the integration time and the

256 number of scans taken in each angular direction were automatically
257 calculated by the software. More specifically, for this study we set
258 the goal of completing an azimuthal lap in approximately one hour
259 (mainly for an easier interpretation of the results and for the
260 subsequent comparison with in-situ instruments of Madrid's air quality
261 monitoring network). Hence, we chose 24 seconds as the maximum exposure
262 time in each angular combination.

263

264 The main advantage of this set-up is that we can observe the
265 daily NO₂ variability over the entire city with a moderate temporal
266 resolution (1-hour). The main disadvantage is that observations for
267 each VAAs averaged over such a short integration period may be affected
268 by microscale phenomena. Nonetheless, NO₂ concentration gradients are
269 particularly strong in space (Borge et al., 2016). Therefore, this
270 exposure time may be well suited to characterize both the azimuthal
271 and the horizontal gradients of NO₂.

272

273 4 Analysis methods

274

275 Using the DOAS technique, the absorptions of the molecular oxygen
276 dimer (O₄) and NO₂ were measured for the entire campaign and for two
277 spectral windows: 352-387 nm (UV region) and 438-487 nm (VIS region).
278 The analysis settings applied for the UV and VIS regions are summarized
279 in Tables 1 and 2, respectively. These configurations follow those
280 used in Wagner et al., 2019.

281

282 Table 1. DOAS spectral settings for the retrieval of O₄ and NO₂ in the
283 UV.

Parameter	Value
-----------	-------

Fitting window	352-387 nm
Wavelength calibration	Based on reference solar atlas (Chance and Kurucz, 2010)
Zenith reference	Scan
Polynomial Order	5
Intensity Offset	Order 2
Shift	The measured spectra and Ring were allowed to shift and stretch (order 1) in wavelength.

Molecule	Cross section
O ₄	293 K (Thalman and Volkamer, 2013)
NO ₂	298 K (Vandaele et al., 1998)
O ₃ a	223 K (Serdyuchenko et al., 2014)
O ₃ b	223 K (Serdyuchenko et al., 2014)
HCHO	297 K (Meller and Moortgat, 2000)
HONO	296 K (Stutz et al., 2000)
Ring_a	Calculated by QDOAS
Ring_b	Ring_a spectrum multiplied by λ^{-4}

285 Table 2. DOAS spectral settings for the retrieval of O₄ and NO₂ in the
 286 VIS.

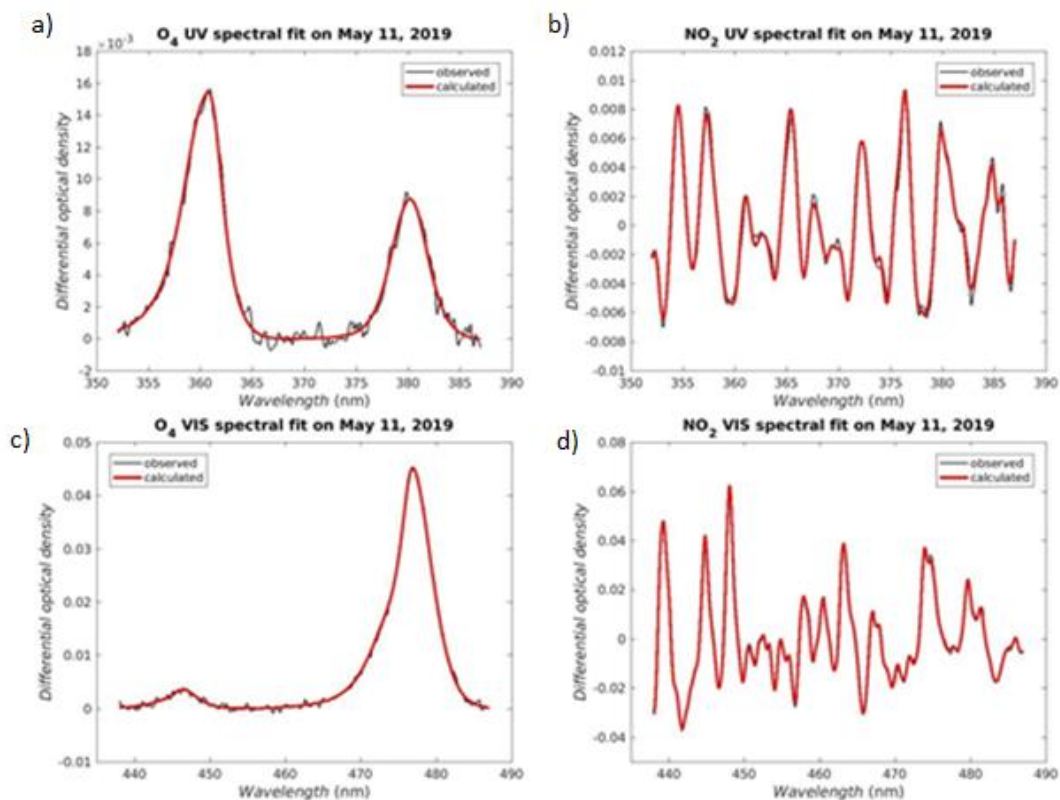
Parameter	Value
Fitting window	438-487 nm
Wavelength calibration	Based on reference solar atlas (Chance and Kurucz, 2010)
Zenith reference	Scan
Polynomial order	5
Intensity offset	Order 2
Shift	The measured spectra and Ring were allowed to shift and stretch (order 1) in wavelength.

Molecule	Cross section
O ₄	293 K (Thalman and Volkamer, 2013)
NO ₂	298 K (Vandaele et al., 1998)
O ₃ a	223 K (Serdyuchenko et al., 2014)
O ₃ b	223 K (Serdyuchenko et al., 2014)
H ₂ O	296 K (Rothman et al., 2010)
Glyoxal	296 K (Volkamer et al., 2005)
Ring a	Calculated by QDOAS
Ring b	Ring a spectrum multiplied by λ^{-4}

287

288 The selected differential absorption cross sections -along with
 289 the spectral window and parameters included in Tables 1 and 2- were
 290 adjusted to the measured differential optical density using the QDOAS
 291 spectral fitting software (developed at BIRA-IASB, [http://uv-
 292 vis.aeronomie.be/software/QDOAS/](http://uv-vis.aeronomie.be/software/QDOAS/)). When the measured DSCD (using
 293 QDOAS) accurately matches the differential optical density for a given
 294 trace gas -i.e. yielding a relatively low residual- there is positive
 295 detection of that trace gas. Figure 3 shows examples of spectral
 296 detection of O₄ and NO₂ for both the UV and VIS regions. Once the DSCDs
 297 are obtained, they are used as input for the profile retrieval
 298 algorithm, as explained in Sect. 4.2.

299



300

301 Figure 3. Spectral detection of O₄ (a) and (c) and NO₂ (b) and (d),
 302 red lines represent the calculated optical densities and black lines
 303 are the measured optical densities.

304

305 4.1 Cloud-screening and quality filtering

306

307 The algorithms for MAXDOAS retrievals of trace gas vertical
308 profiles are based on estimating the light paths (along with their
309 corresponding scattering probability) for a clear sky day. A
310 significant cloud cover could noticeably impact the calculations,
311 mainly because of multiple scattering effects, adding large
312 uncertainties to the retrieval process. For this reason, the set of
313 measured spectra has to be cloud-screened, filtering out those spectra
314 affected by clouds. In order to achieve that, we used the cloud-free
315 AERosol RObotic NETwork (AERONET) database. AERONET is a global network
316 of ground-based remote sensing instruments established by NASA and
317 PHOTONS (https://aeronet.gsfc.nasa.gov/new_web/index.html) to measure
318 aerosols and their optical, microphysical and radiative properties.
319 The AERONET instruments provide a long-term, continuous and readily
320 accessible public domain database of aerosol measurements worldwide.
321 These databases are reported with three quality levels, in particular,
322 we used the Level 2.0 (cloud-screened and quality-assured) database
323 provided by the AERONET instrument placed in Madrid. This information
324 is combined with the photos taken by the camera installed on the
325 MAXDOAS. As mentioned in Sect. 3.1, this webcam points at the same
326 azimuthal direction as the light collector, therefore we had a set of
327 azimuthal photos of the sky for each horizontal lap. We estimated the
328 cloud cover using a code that gets the RGB coordinates -the three
329 chromaticities of the blue, green and red- and it changes them into LCh
330 coordinates -L indicates lightness, C represents chroma and h is the
331 hue angle. Based on criteria of luminosity, colour and saturation, the
332 code estimates the cloud index.

333

334 Since we are dealing with a non-linear, least-squares system of
335 equations, there is a notable gradient concerning the quality and
336 uncertainties in the results. Hence, before proceeding with the
337 profiling algorithm, several quality filters were applied to the DSCDs:
338 firstly, every DSCD that yielded either a relative uncertainty larger

339 than 1 or a residual Root Mean Square (RMS) higher than 0.01 (in
340 optical density units) was rejected. After that, we estimated the
341 DSCDs detection limit for a given trace gas as the ratio of the
342 residual RMS (in optical density units) associated to each DSCD and
343 the maximum value of the differential cross section of that trace gas.
344 Then, we discarded the DSCDs that had an absolute value lower than
345 twice the derived detection limit (a similar approach was carried out
346 in Peters et al., 2012). Finally, we used the daily plus/minus three
347 standard deviation criterion that AERONET applies for its cloud-
348 filtered data, keeping the DSCD that falls within plus/minus three
349 standard deviations from each daily mean. Overall, the number of
350 MAXDOAS DSCDs cycles that were considered valid after the quality
351 checks was slightly above 90 % for both trace gases and spectral
352 regions.

353

354 4.2 Inversion algorithm and vertical profiles

355

356 We applied an inversion algorithm method to the measured DSCDs
357 to estimate the light paths and subsequently derive the trace gas
358 vertical concentration profile. The main idea behind these inversion
359 algorithms is based on the fact that each VEA has different scattering
360 heights and light paths (Solomon et al., 1987). Therefore, a given set
361 of measured DSCDs contains information about the vertical distribution
362 of a certain trace gas. Since higher VEAs are generally related to
363 higher scattering heights, different layers within the atmosphere can
364 be sampled, especially in the lower troposphere. The forward models
365 that calculate these scattering events are called Radiative Transfer
366 Models (RTMs), and they study the transport of radiation as well as
367 its interaction with matter. Each inversion algorithm needs a forward
368 model that simulates the atmosphere in order to estimate the light
369 paths and retrieve the vertical profiles of trace gases. There are
370 several inversion algorithms for atmospheric applications, but for

371 this work we have used the bePRO inversion algorithm, developed at
372 BIRA-IASB (Clémer et al., 2010). The original calculation was built
373 based on the Optimal Estimation Method (OEM; Rodgers, 2000) and it
374 comprises two steps: first, the light paths and the vertical profiles
375 of irradiance extinction are calculated using the O_4 DSCDs; then, the
376 target trace gas vertical concentration profile is retrieved using the
377 corresponding light paths and measured absorption. In order to do
378 that, bePRO simulates the atmospheric state characterizing several
379 different physical phenomena including pressure and temperature
380 vertical profiles, Rayleigh and Mie scattering events (along with
381 their respective phase functions), the effect of the surface albedo,
382 the light path geometries or the irradiance extinction processes. Once
383 the atmospheric vector state is defined, its combination with a certain
384 vertical concentration profile results in the simulated DSCDs. This
385 vertical profile is iterated until the generated set of simulated
386 DSCDs is optimized with respect to the measured DSCDs so that the
387 residual is minimized. As a result, an optimal vertical profile is
388 obtained when the iteration is finished for each MAXDOAS cycle.

389

390 The measured O_4 DSCDs are used to estimate the light paths for
391 each VEA since they are related to the square of the atmospheric O_2
392 profiles, which are well-known. This profile is fairly steady during
393 the day and does not heavily depend on chemistry factors. Therefore,
394 the measured O_4 DSCDs can provide information on the irradiance
395 extinction in the atmosphere. This extinction profile is usually
396 associated with the aerosol extinction coefficients and thus, its
397 vertical integration yields the Aerosol Optical Depth (AOD). These
398 aerosol extinction profiles are required to subsequently evaluate
399 trace gas profiles since they strongly affect the relative light paths
400 and hence the concentration profiles derived from them.

401

402 Once the light paths are computed in the previous step, and with
403 the purpose of best simulating the measured DSCDs, a linear analysis
404 process is performed for the measured DSCDs of the target trace gas,
405 yielding the optimal vertical concentration profile. The vertical
406 integration of this concentration profile is called the Vertical Column
407 Density (VCD).

408

409 The retrieval consists of an iterative, nonlinear system of
410 equations, and hence there is no unique solution. This means that an
411 a priori profile is needed, both for starting the iterations and to
412 avoid the final solution to be non-realistic (i.e. with no physical
413 meaning). In order to construct these a priori profiles we used
414 exponentially decreasing curves as follows:

415

$$416 \quad ap(z) = \frac{VC_i}{sh} \exp\left(\frac{-z}{sh}\right) \quad (2)$$

417

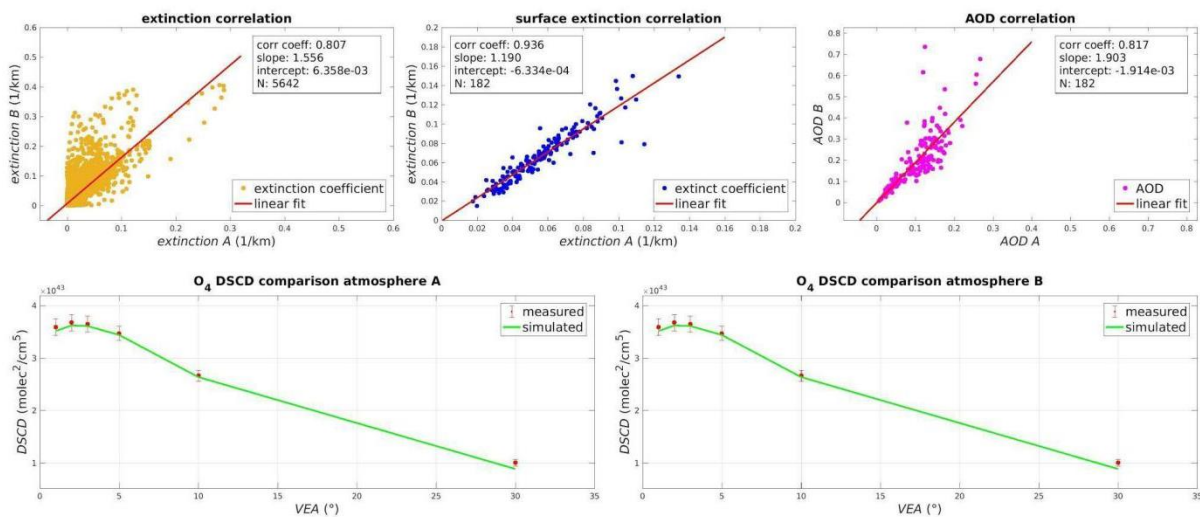
418 where $ap(z)$ is the a priori vertical profile at a certain
419 altitude z , VC_i is the vertical integration of the profile for the
420 MAXDOAS cycle i and sh is the scaling height constant. We used 0.5
421 km as the scaling height constant for all the a priori profiles
422 (Hendrick et al., 2014). Regarding the VC, we assumed an AOD of 0.05
423 for the O_4 retrieval, while for NO_2 we applied the geometrical
424 approximation followed in Hönninger et al., 2004, taking the measured
425 DSCD at VEA 30° for every MAXDOAS cycle. This approximation assumes
426 that most of the absorption events are located below the scattering
427 height.

428

429 With respect to the remaining atmospheric parameters, we chose
430 typical values for urban environments: surface albedo of 0.07,
431 correlation length of 0.4 km and an a priori covariance factor of 1
432 (see Hendrick et al., 2014). We use the air number density vertical

433 profile since it is directly related to the number of O_4 absorptions,
 434 and therefore to the O_4 DSCDs. Hence the relative differences,
 435 particularly for lower VEAs, between the measured and simulated O_4
 436 DSCDs are usually assigned to aerosol extinction. Note however, as
 437 shown below, that uncertainties in the air number density profiles -
 438 arising from uncertainties in the values or shape of the temperature
 439 and pressure profiles- could also explain such differences (Fig. 4).

440



441

442 Figure 4. Comparison of retrieved aerosols using two different
 443 atmospheric profiles: the US Standard (atmosphere A) and the US
 444 Standard adapted to the altitude above sea level of Madrid (atmosphere
 445 B).

446

447 Here we compare the simulation of O_4 DSCDs using two different
 448 sets of atmospheric profiles: i) the US Standard, and ii) the same
 449 profile but interpolating the pressure profile to Madrid's height
 450 above sea level (mean value of 667 m). This means that the temperature
 451 profile is assumed to be the same but the pressure profile is shifted
 452 less than 10%, so there are no major variations within the profiles.
 453 The lower row in Fig. 4 shows that both atmospheric profiles result
 454 in almost the same set of simulated O_4 DSCDs, however the aerosol

455 extinction coefficients differ significantly (although less for the
456 surface layer coefficients), and consequently, the AOD also varies.
457 From this we infer that:

458

459 i) the retrieval is mainly driven by the measured DSCDs, which
460 leaves a relatively low weight for the chosen atmospheric
461 profiles (pressure and temperature). Therefore, we can
462 obtain consistent correlations between the measured and
463 simulated O_4 DSCDs.

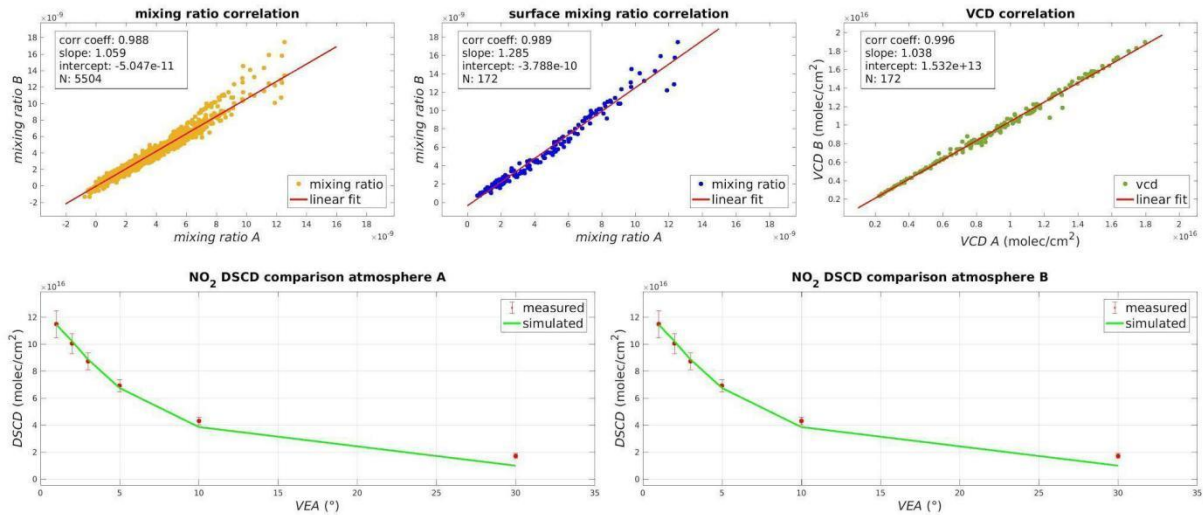
464

465 ii) we cannot reliably assign the extinction coefficients at
466 each layer to aerosols (especially for atmospheric layers
467 above the surface layer), but rather consider them as
468 irradiance extinction coefficients.

469

470 Furthermore, we have assessed the impact of the pressure and
471 temperature profiles choice on the trace gas retrieval. As can be
472 noted in Fig. 5, there is no significant effect coming from this choice
473 on the simulated NO_2 DSCDs. These are basically the same (and with
474 very good agreement with the measured DSCDs), as well as the derived
475 concentration coefficients and their integration (VCD).

476



477

478 Figure 5. NO₂ retrieval comparison using two different atmospheric
 479 profiles: the US Standard (atmosphere A) and the US Standard adapted
 480 to the altitude above sea level of Madrid (atmosphere B).

481

482 However, we also evaluate if a similar behavior can be expected
 483 for larger variations in the pressure and temperature profiles. We
 484 first obtained the average surface temperature and pressure values for
 485 the duration of the campaign (May-July, 2019). With the inclusion of
 486 these values in the retrieval, we found that, within the first 10 km
 487 height, the RMS of the relative variations with respect to the standard
 488 atmosphere were about 8 %. Although it is a small change, it is indeed
 489 not negligible. Nonetheless, when evaluating light paths, the relative
 490 changes were below 2%. Therefore, here we use the US Standard
 491 atmospheric profiles for the NO₂ retrievals.

492

493 Table 3 summarizes the average uncertainties (using one standard
 494 deviation for each component) of the retrieval, along with their
 495 relative contributions, for the ground layer (0-200 m height). he
 496 mean, overall uncertainty for NO₂ in both spectral regions is in the
 497 order of 10%.

498

499 Table 3. Summary of average uncertainties of the retrieval in both
500 spectral regions.

Variable \ Trace gas	NO ₂ UV (%)	NO ₂ VIS (%)
Irradiance Extinction	7.7	5.1
DSCD	4.8	3.2
Surface Mixing Ratio	5.0	8.7
Total	10	11

501

502 4.3 Estimation of NO₂ horizontal gradients

503

504 Making use of the different paths that photons travel through
505 the atmosphere for different wavelengths, we can estimate the
506 horizontal distribution of NO₂. We use the estimated horizontal light
507 paths at two wavelengths, 360.8 nm and 477 nm, for the surface layer
508 (0-200 m height). The different light paths at 360.8 and 477 nm provide
509 information about the horizontal distribution of NO₂ mixing ratios
510 within the surface layer. In order to evaluate these horizontal paths,
511 we have used our own codes that implement the RTM equations based on
512 previous pioneering work (Solomon et al., 1987). These equations yield
513 a vector of scattering events along with their respective
514 probabilities. If we take a VEA of 0 degrees (i.e. horizontal viewing),
515 then the scalar product of such vectors produces the length of the
516 horizontal light path. We computed this for every MAXDOAS cycle and
517 for both wavelengths, yielding typical -representative- horizontal
518 distances of about 8-10 km for the UV (at 360.8 nm) and between 15-20
519 km for the VIS window (at 477 nm). The next step follows the “onion-
520 peeling” approach proposed by Ortega et al. 2015 (the strong dependence
521 of scattering with wavelength means that shorter wavelengths result
522 in shorter light paths). We assign the UV (i.e. 360.8 nm) mixing ratios

523 (mr_{uv}) and their expected horizontal paths (d_{uv}) to the first peel
 524 (mr_A , meaning zone A). Then the second peel (zone B, mr_B) can be
 525 derived as:

526

$$527 \quad mr_B = \frac{mr_{vis} \times d_{vis} - mr_{uv} \times d_{uv}}{d_{vis}} \quad (3)$$

528

529 Thereby, deriving mixing ratios (mr_a and mr_b) representative of two
 530 different horizontal distances for each VAA.

531

532 5 Results

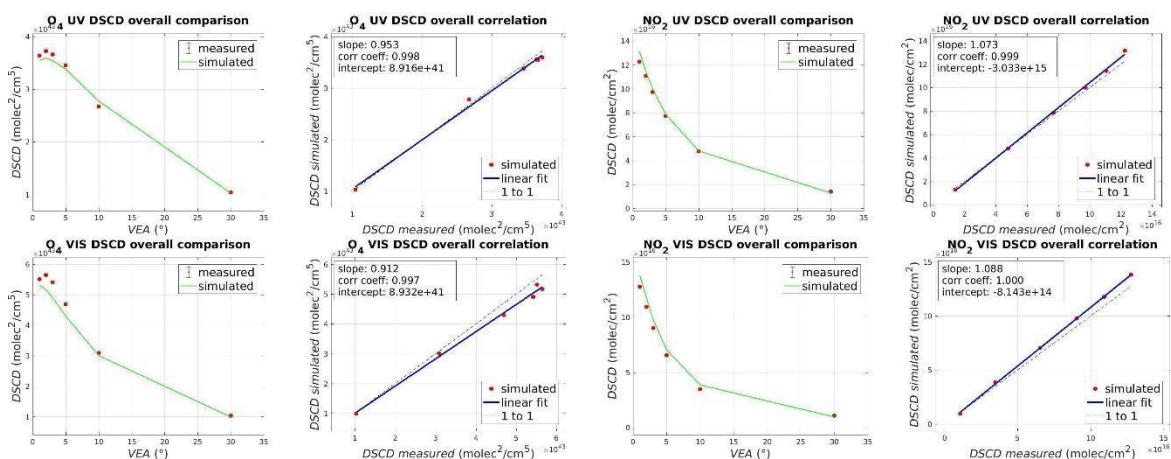
533

534 5.1 O₄ and NO₂ DSCDs assessment

535

536 Once the vertical profiles are retrieved using the RTM explained
 537 in Sect. 4, we compare the set of simulated DSCDs predicted by the
 538 model with the measured DSCDs coming from the absorption analysis. An
 539 estimation of the overall goodness of the profile retrieval comes from
 540 the correlation between the measured and simulated DSCDs for the entire
 541 campaign (Fig. 6).

542



543

544 Figure 6. Comparison between simulated and measured DSCDs of O₄ and
545 NO₂.

546

547 The fit between the measured and the simulated DSCDs shows
548 correlations (r^2) very close to 1 for both O₄ and NO₂ in the UV and VIS
549 regions. As mentioned before, the inverse retrieval finds the optimal
550 solution of the vertical concentration profile that generates the best
551 set of simulated DSCDs.

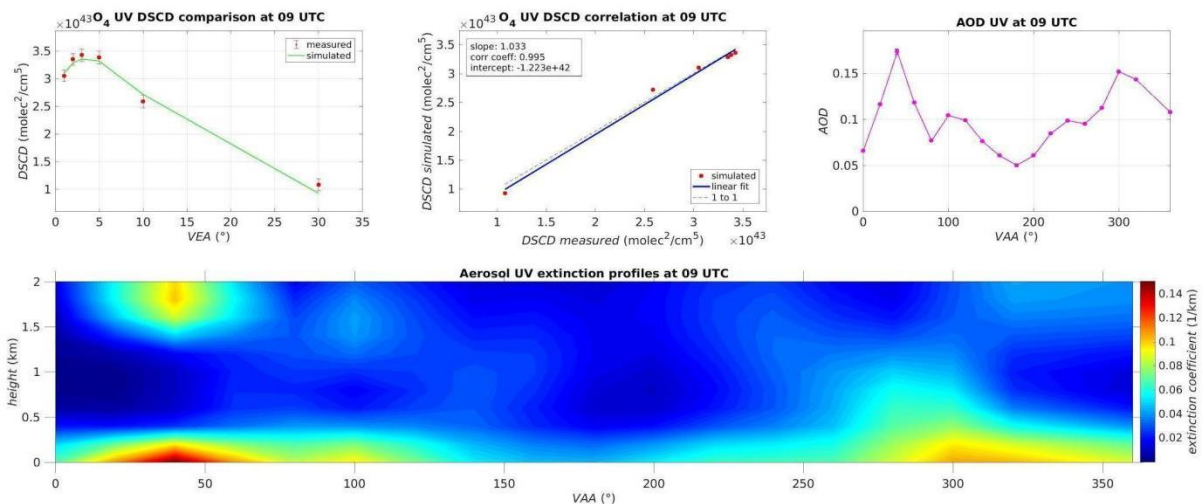
552

553 5.2 Two-dimensional maps

554

555 We now combine the VAA and height for each azimuthal cycle of
556 the MAXDOAS-2D to generate a two-dimensional concentration map. Fig.
557 7 shows an example of the O₄ retrieval in the UV for a given azimuthal
558 cycle. In addition to the profiles, Fig. 7 also shows the comparison
559 and correlation of measured and simulated DSCDs for that azimuthal
560 cycle, along with the evolution of retrieved AOD. The AOD varies
561 between 0.05 and 0.18 within this azimuthal cycle (Fig. 7, upper
562 panel). The contour plot shows the irradiance extinction coefficient
563 profiles with maximum values of 0.14 km⁻¹ (near the ground and at around
564 40° VAA) associated with aerosol extinction (see discussion in Sect.
565 4.2). Note the enhanced extinction at about 2 km height pointing at
566 50 VAA. This could be due to particulate matter emitted by traffic
567 (there is a main road at that location) (Carnerero et al., 2018).
568 Further research is needed to better establish the vertical
569 distribution of aerosols in Madrid, and their diurnal evolution.

570



571

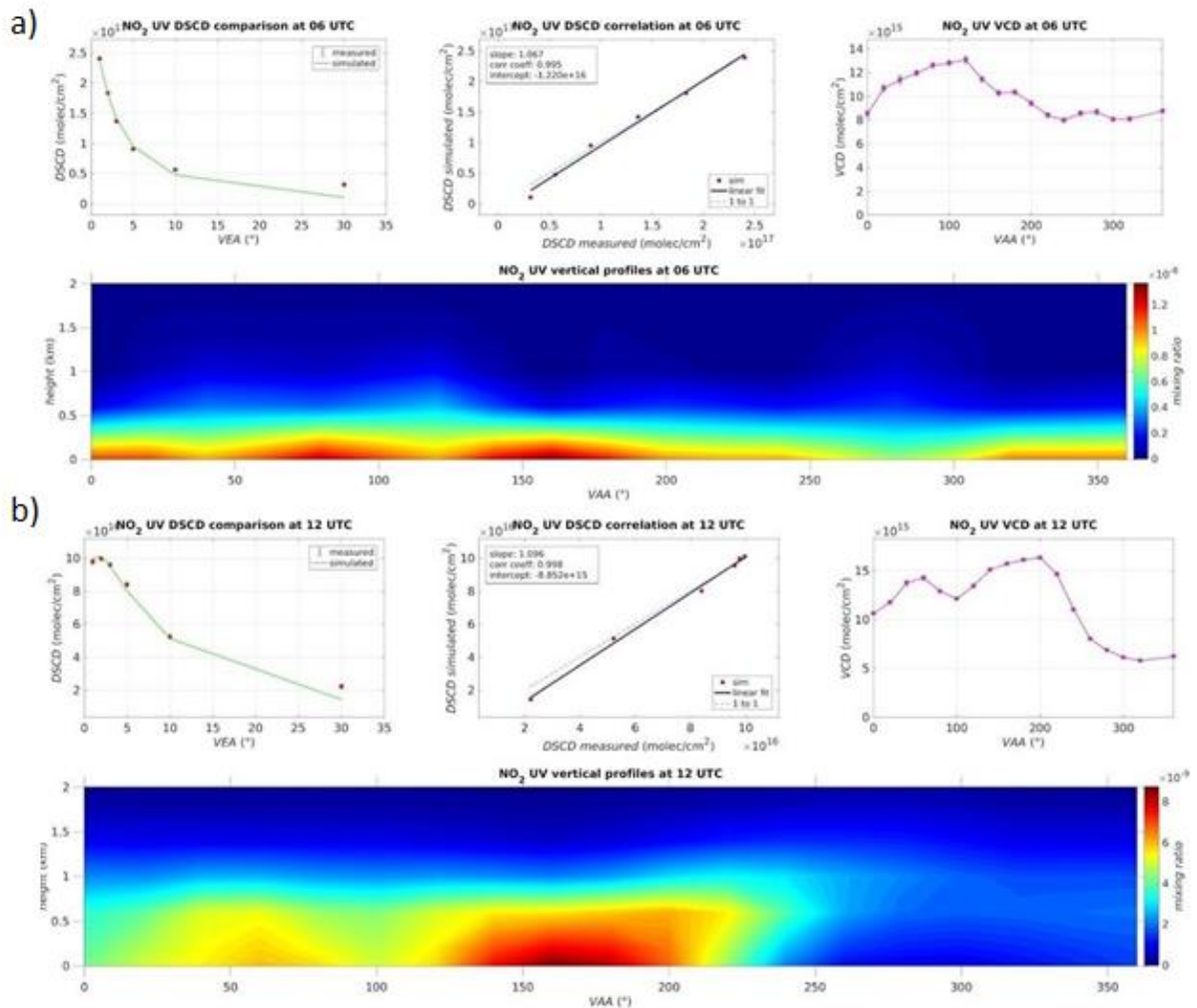
572 Figure 7. Example of O_4 and AOD retrievals in the UV region at 9
 573 UTC on May 11, 2019. These contour plots are smoothed from adjacent
 574 VAA data points separated by 20° in order to estimate the azimuthal
 575 distribution of the irradiance extinction coefficients over Madrid.

576

577 Figure 8 presents a two-dimensional representation of NO_2 on May
 578 11, 2019 at two different hours (6 UTC and 12 UTC, respectively). Both
 579 contour plots show maximum NO_2 values of 12 ppbv at 6 UTC and 8 ppbv
 580 at 12 UTC, when the instrument is pointing south (i.e. VAA of 180°).
 581 We chose to show this day as an example since it was a clear sky day
 582 and yielded NO_2 mixing ratios that were representative of the entire
 583 period of measurements. These values correspond to the layer near the
 584 ground and are in good agreement with our previous MAXDOAS observations
 585 in Madrid (Garcia-Nieto et al., 2018). The retrieved azimuthal
 586 distribution of NO_2 agrees with previous reports that show higher
 587 pollution levels in the southern section of Madrid (Picornell et al.,
 588 2019). NO_2 VCDs range from 5×10^{15} molecules cm^{-2} (at 12 UTC and pointing
 589 at 300° VAA) up to 15×10^{15} molecules cm^{-2} (at 12 UTC and pointing at
 590 200° VAA), with an average value of 1×10^{16} molecules cm^{-2} . Although
 591 there can be different NO_x emission rates at both times of the day (6
 592 and 12 UTC), the increase in the boundary layer height during the day
 593 could explain the similar values of VCDs at both hours but generally
 594 lower surface mixing ratios at 12 UTC. Note that NO_2 is efficiently

595 mixed within the boundary layer as it develops during the day (i.e.
 596 boundary layer height usually lags the solar zenith angle) (Fig. 8)
 597 (de la Paz et al., 2016).

598



599

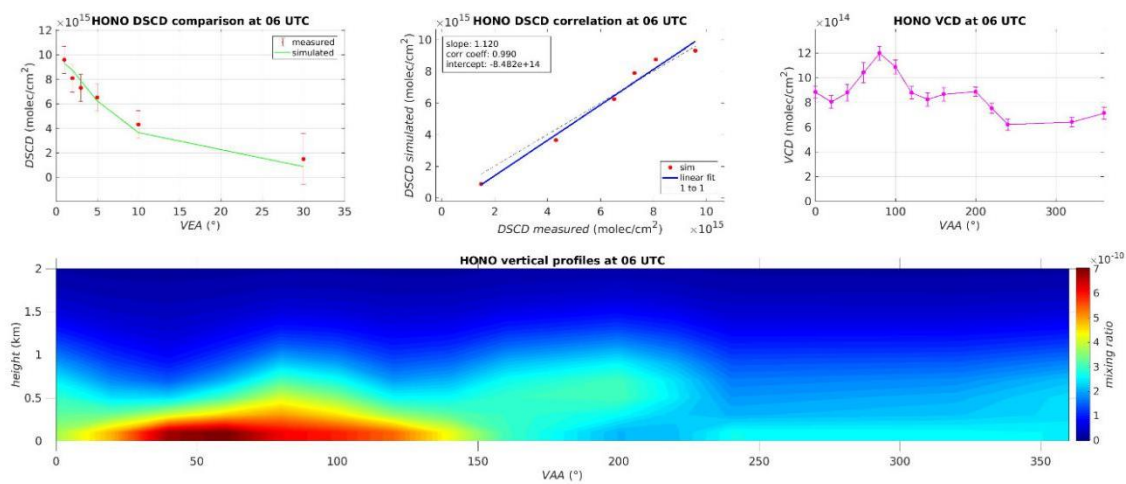
600 Figure 8. NO₂ vertical distribution retrieved in the UV region at 6
 601 UTC (a) and at 12 UTC (b) on May 11, 2019. These contour plots are
 602 smoothed from adjacent VAA data points separated by 20° in order to
 603 estimate the azimuthal distribution of NO₂ over Madrid.

604

605 We have also analyzed HONO DSCDs measured by the MAXDOAS-2D using
 606 the same configuration as in Garcia-Nieto et. al., 2018. Figure 9
 607 shows a two-dimensional representation of HONO on May 11, 2019 at 6
 608 UTC. We retrieve surface layer peak values of 0.7 ppbv pointing at 50°

609 of VAA in the early morning, in agreement with previous studies for
 610 HONO in urban environments (see Hendrick et al., 2014; Ryan et al.,
 611 2018). The VCDs at 6 UTC range from 6×10^{14} to 1.2×10^{15} molecule cm^{-2} .
 612 The combination of spatially distributed measurements of NO_2 and HONO
 613 can be used together with chemical transport models to further
 614 understand pollution dynamics in Madrid.

615



616

617 Figure 9. HONO vertical distribution retrieved in the UV region at 6
 618 UTC. These contour plots are smoothed from adjacent VAA data points
 619 separated by 20° in order to estimate the azimuthal distribution of
 620 HONO over Madrid.

621

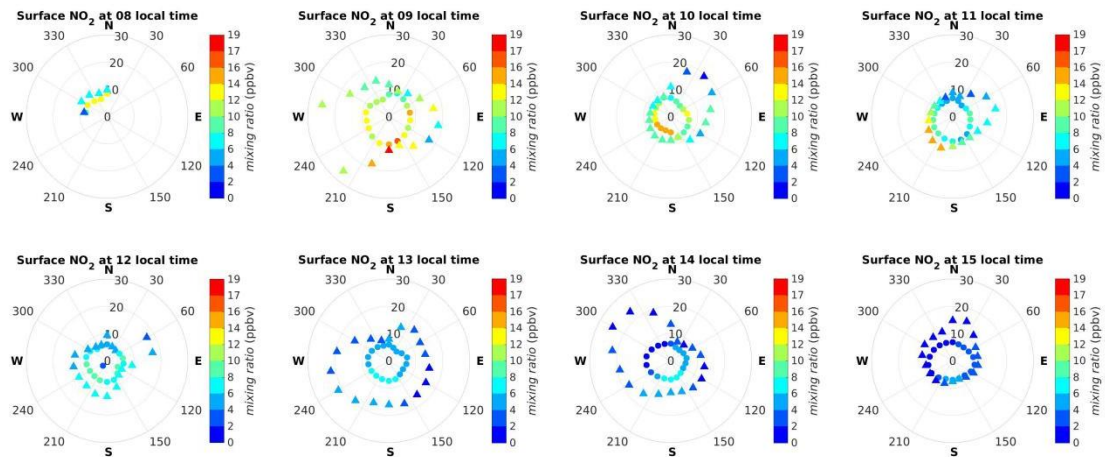
622 5.3 Horizontal distribution of NO_2

623

624 Based on Eq. (3), we derive the horizontal distribution of NO_2
 625 in the surface layer (0-200 m height). Figure 10 shows an example of
 626 surface layer NO_2 mixing ratios over two radial distances from the
 627 MAXDOAS-2D instrument (using the UV and the VIS NO_2 , respectively, as
 628 explained in Section 4.3), located at the center of the plot. The
 629 highest mixing ratios occur during the first sunlit hours (7-8 UTC),
 630 coincident with the morning peak of NO_x emissions in Madrid (Quassdorff
 631 et al., 2016). This early morning peak is followed by a gradual

632 decrease in surface layer NO₂ mixing ratios during the day. Note that
633 NO₂ is predominantly located in the southern part of the semisphere
634 (VAA from 90° to 270°).

635



636

637 Figure 10. Polar plots of NO₂ within the surface layer (0-200 m height)
638 for May 11, 2019. Please note that these polar plots extend over a
639 direction perpendicular to those shown in Fig. 8. Here, circles are
640 used for the UV (shorter horizontal light path) and triangles for the
641 VIS (larger horizontal light path).

642

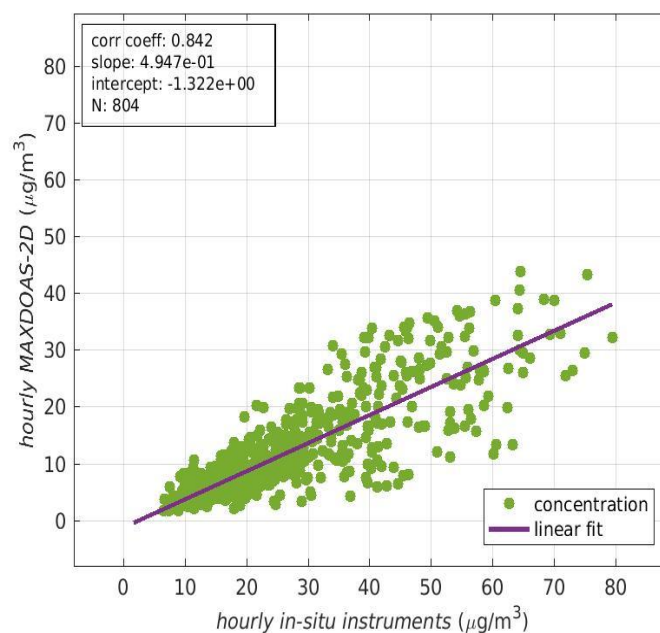
643 5.4 Correlation with Madrid's in-situ air quality monitoring stations

644

645 We suggest that MAXDOAS-2D mesoscale observations may complement
646 the information provided by the local air quality monitoring network
647 based on reference analytical techniques (according to Directive
648 2008/50/EC). While air quality monitors of the reference network
649 provide information about ambient concentrations in their specific
650 locations (currently 24 air quality monitoring stations measure NO₂
651 within the city, see AM, 2019), MAXDOAS-2D observations produce near
652 ground-level concentrations averaged over the optical path in a given
653 direction. That prevents us from quantitatively comparing both types

654 of observations. Nonetheless, we analyzed their correspondence using
655 the NO₂ concentrations measured by the in-situ instruments throughout
656 the entire city, and the NO₂ mixing ratios within the surface layer
657 derived from our MAXDOAS-2D instrument over the 2-month period (May-
658 June, 2019). For this comparison, we considered the air quality
659 monitoring stations within a distance from the MAXDOAS-2D equal or
660 lower than 10 km. Since this is the typical horizontal light path for
661 the UV region, we decided to include only the NO₂ values retrieved in
662 the UV region for the comparison. Strong gradients between the values
663 measured by the in-situ instruments are typical. Therefore, and
664 considering that we are mainly interested in their temporal correlation
665 with respect to our MAXDOAS-2D measurements, we compare both the in-
666 situ NO₂ and surface layer MAXDOAS-2D hourly-averaged data. Note that
667 for the MAXDOAS-2D this approximately corresponds to averaging the
668 surface layer values for each azimuthal lap, given that each azimuthal
669 lap takes approximately 1 hour to complete.

670



671

672 Figure 11. Correlation between in-situ observations from Madrid's air
673 quality monitoring network and those derived from the MAXDOAS-2D

674 instrument for the surface layer (0-200 m height).

675

676 Despite the different spatial representativeness, Figure 11 shows
677 a reasonably good correlation coefficient of 0.842 between both
678 datasets for the two-month campaign. The slope is lower than 1, this
679 can be explained by the typical NO₂ vertical profiles in urban
680 environments. Simulations performed over Madrid with a high-resolution
681 Eulerian air quality model (Borge et al., 2018) yielded an
682 exponentially decreasing with height NO₂ profile. Therefore, the
683 MAXDOAS-2D mixing ratios, which represent an average across the surface
684 layer (0-200 m height), are not expected to quantitatively match the
685 values of in-situ instruments, located close to the surface (between
686 0-10 m height). Similar conclusions -and slopes comparable to the one
687 retrieved above- regarding the correlation between in-situ and MAXDOAS
688 instruments can be found in previous works (Schreier et al., 2019;
689 Kramer et al., 2008; Chan et al., 2020). In addition, there is a good
690 temporal correlation between in-situ and MAXDOAS-2D measurements over
691 an extended period of time.

692

693 6 Summary and Conclusions

694

695 An analysis of O₄, NO₂ and HONO vertical concentration profiles
696 in the urban atmosphere of Madrid (Spain) has been performed over two
697 months (from May 6 to July 5, 2019). We analyzed the absorptions and
698 derived the corresponding DSCDs for both trace gases in the UV and VIS
699 regions. Then, the corresponding profiles were retrieved using a RTM.
700 In this step, we assessed the impact of different atmospheric profiles
701 (pressure and temperature) in the retrieval results, and found that
702 the set of chosen atmospheric profiles has a small impact on the O₄
703 retrieval and the estimation of light paths. However, there is a
704 noticeable change in the irradiance extinction profiles, which makes

705 difficult to quantitatively assign extinction due to aerosols,
706 especially in heights above the boundary layer.

707 The overall comparison of measured and simulated trace gas DSCDs
708 showed that they were in very good agreement (with correlation
709 coefficients close to 1), supporting the reliability of the
710 observations. The MAXDOAS-2D instrument provides the first two-
711 dimensional view (in height and VAA) of pollution concentration in the
712 city of Madrid. Exploring one day (May 11, 2019) we compared two hours:
713 the peak rush hour and noon time, obtaining NO₂ maximum values of 12
714 ppbv and 8 ppbv respectively, both maxima pointing to the south
715 direction. Two-dimensional HONO measurements were also made with
716 mixing ratio peaks of 0.7 ppbv in the early morning, and VCDs ranging
717 from 6×10^{14} to 1.2×10^{15} molecule cm⁻².

718

719 We have also inferred information on the horizontal gradient of
720 NO₂ within the surface layer making use of the strong dependence
721 between wavelengths and light paths across the NO₂ absorption spectrum.
722 The resulting “onion-peeling” figures indicate peak values of NO₂ in
723 the early morning and in the southern section of the city (around 180
724 ° VAA), it resulted in a gradual decrease in NO₂ mixing ratios during
725 the day, maximum values of NO₂ appear in the southern part of the
726 semisphere. Finally, we suggest that the new mesoscale information
727 provided by the MAXDOAS-2D instrument helps in the study of pollution
728 transport dynamics. MAXDOAS-2D and in-situ instruments provide
729 different information, and thus, combining both can improve our
730 understanding of the complex issue of air pollution in the city of
731 Madrid.

732

733 Author Contribution

734

735 A.S-L. devised the research. D.G-N. and N.B. carried out the
736 measurements and analyzed the data. D.G-N., N.B., R.G. and A.S-L.
737 analyzed and interpreted the results. D.G-N. wrote the manuscript with
738 contributions from all co-authors.

739

740 Acknowledgements

741

742 The authors want to thank Manuel Perez and David Armenteros for
743 technical assistance with the instrument, and David de la Paz for
744 model assistance. This work was supported by the TECNAIRE project
745 (“Técnicas innovadoras para la evaluación y mejora de la calidad del
746 aire urbano”) S2013/MAE-2972. We would also like to thank Juan Ramón
747 Moreta González (PI) and his staff for establishing and maintaining
748 the AERONET sites in Madrid used in this investigation. We acknowledge
749 support of the publication fee by the CSIC Open Access Publication
750 Support Initiative through its Unit of Information Resources for
751 Research (URICI)

752

753 References

754

755 Ayuntamiento de Madrid (AM): Madrid 2016 Annual Air Quality Assessment
756 Report (Calidad del aire Madrid 2019). General Directorate of
757 Sustainability and Environmental Control, Madrid City Council
758 Available online -only Spanish version- at
759 http://www.mambiente.munimadrid.es/opencms/export/sites/default/calibre/Anexos/Memorias/Memoria_2019.pdf, 2019.

761

762 Benavent, N., Garcia-Nieto, D., Wang, S., & Saiz-Lopez, A.: MAX-DOAS
763 measurements and vertical profiles of glyoxal and formaldehyde in
764 Madrid, Spain. Atmospheric Environment, 199, 357-367, 2019.

765

766 Borge, R., Narros, A., Artinano, B., Yagüe, C., et al.: Assessment of
767 micro- scale spatio-temporal variation of air pollution at an urban
768 hotspot in Madrid (Spain) through an extensive field campaign. *Atmos.*
769 *Environ.* 140, 432-445, 2016.

770

771 Borge, R., Santiago, J. L., de la Paz, D., Martín, F., Domingo, J.,
772 Valdés, C., Sánchez, B., Rivas, E., Rozas, M. T., Lázaro, S., Pérez,
773 J., & Fernández, Á.: Application of a short term air quality action
774 plan in Madrid (Spain) under a high-pollution episode - Part II:
775 Assessment from multi-scale modelling. *Science of the Total*
776 *Environment*, 635, 1574-1584.
777 <https://doi.org/10.1016/j.scitotenv.2018.04.323>, 2018.

778

779 Carnerero, C., Pérez, N., Reche, C., Ealo, M., Titos, G., Lee, H.-K.,
780 Eun, H.-R., Park, Y.-H., Dada, L., Paasonen, P., Kerminen, V.-M.,
781 Mantilla, E., Escudero, M., Gómez-Moreno, F. J., Alonso-Blanco, E.,
782 Coz, E., Saiz-Lopez, A., Temime-Roussel, B., Marchand, N., Beddows,
783 D. C. S., Harrison, R. M., Petäjä, T., Kulmala, M., Ahn, K.-H.,
784 Alastuey, A., and Querol, X.: Vertical and horizontal distribution of
785 regional new particle formation events in Madrid, *Atmos. Chem. Phys.*,
786 18, 16601-16618, <https://doi.org/10.5194/acp-18-16601-2018>, 2018.

787

788 Chan, K. L., Wiegner, M., Alberti, C., & Wenig, M.: MAX-DOAS
789 measurements of tropospheric NO₂ and HCHO in Munich and the comparison
790 to OMI and TROPOMI satellite observations. *Atmospheric Measurement*
791 *Techniques Discussions*, 2020.

792

793 Chance, K., Kurucz, R.L.: An improved high-resolution solar reference
794 spectrum for earth's atmosphere measurements in the ultraviolet,
795 visible, and near infrared. *J. Quant. Spectrosc. Radiat. Transf.*;

796 Special Issue Dedicated to Laurence S. Rothman on the Occasion of his
797 70th Birthday 111 (9), 1289-1295, 2010.

798

799 Clémer, K., Van Roozendael, M., Fayt, C., Hendrick, F., Hermans, C.,
800 Pinardi, G., Spurr, R., Wang, P., De Mazière, M.: Multiple wavelength
801 retrieval of tropospheric aerosol optical properties from MAXDOAS
802 measurements in Beijing. Atmospheric Measurement Techniques 3 (4),
803 863, 2010.

804

805 Cuevas, C., Notario, A., Adame, J. Hilboll, A., Richter, A., Burrows,
806 J.P, Saiz-Lopez, A.: Evolution of NO₂ levels in Spain from 1996 to
807 2012. Sci Rep 4, 5887, 2014.

808

809 de la Paz, D., Borge, R., & Martilli, A.: Assessment of a high
810 resolution annual WRF-BEP/CMAQ simulation for the urban area of Madrid
811 (Spain). Atmospheric Environment, 144, 282-296.
812 <https://doi.org/10.1016/j.atmosenv.2016.08.082>, 2016.

813

814 Dimitropoulou, E., Hendrick, F., Pinardi, G., Friedrich, M., Merlaud,
815 A., Tack, F., De Longueville, H., Fayt, C., Hermans, C., Laffineur,
816 Q., Fierens, F., & Van Roozendael, M.: Validation of TROPOMI
817 tropospheric NO₂ columns using dual-scan MAX-DOAS measurements in
818 Uccle, Brussels. Atmospheric Measurement Techniques Discussions, 2020.

819

820 European Environment Agency (EEA).: Air quality in Europe - 2019
821 report. EEA Technical Report No 10/2019. ISBN: 978-92-9480-088-6.
822 Available online at: [http://www.eea.europa.eu/publications/air-](http://www.eea.europa.eu/publications/air-quality-in-europe-2019)
823 [quality-in-europe-2019.](http://www.eea.europa.eu/publications/air-quality-in-europe-2019), 2019

824

825 Hendrick, F., Müller, J.-., Clémer, K., Wang, P., De Mazière, M., Fayt,
826 C., Gielen, C., Hermans, C., Ma, J., Pinardi, G., Stavrakou, T.,
827 Vlemmix, T., Van Roozendael, M.: Four years of ground-based MAX-DOAS
828 observations of HONO and NO₂ in the Beijing area. *Atmos. Chemical*
829 *Physics*, 14 (2), 765, 2014.

830

831 Garcia-Nieto, D., Benavent, N., Saiz-Lopez, A.: Measurements of
832 atmospheric HONO vertical distribution and temporal evolution in
833 Madrid (Spain) using the MAXDOAS technique. *Science of the Total*
834 *Environment*. 643, 957-966, 2018.

835

836 Hönninger, G., von Friedeburg, C., Platt, U.: Multi axis differential
837 optical absorption spectroscopy (MAXDOAS). *Atmos. Chem. Phys.* 4 (1),
838 231-254, 2004.

839

840 Izquierdo, R., García Dos Santos, S., Borge, R., Paz, D. de la,
841 Sarigiannis, D., Gotti, A., & Boldo, E.: Health impact assessment by
842 the implementation of Madrid City air-quality plan in 2020.
843 *Environmental Research*, 183, 109021, 2020.

844

845 Kramer, L. J., Leigh, R. J., Remedios, J. J., & Monks, P. S: Comparison
846 of OMI and ground-based in situ and MAX-DOAS measurements of
847 tropospheric nitrogen dioxide in an urban area. *Journal of Geophysical*
848 *Research Atmospheres*, 2008.

849

850 Meller, R., Moortgat, G.K.: Temperature dependence of the absorption
851 cross sections of formaldehyde between 223 and 323 K in the wavelength
852 range 225-375 nm. *Journal of Geophysical Research: Atmosphere* 105,
853 7089-7101, 2009.

854

855 Monks, P. S., Granier, C., Fuzzi, S., Stohl, A., Williams, M. L.,
856 Akimoto, H., Amann, M., Baklanov, A., Baltensperger, U., Bey, I., Blake,
857 N., Blake, R. S., Carslaw, K., Cooper, O. R., Dentener, F., Fowler,
858 D., Fragkou, E., Frost, G. J., Generoso, S., ... von Glasow, R.:
859 Atmospheric composition change - global and regional air quality.
860 Atmospheric Environment, 43(33), 5268-5350.
861 <https://doi.org/10.1016/j.atmosenv.2009.08.021>, 2009.

862

863 Ortega, I., Koenig, T., Sinreich, R., Thomson, D., Volkamer, R.: The
864 CU 2-D-MAX-DOAS instrument - Part 1: Retrieval of 3-D distributions
865 of NO₂ and azimuth-dependent OVOC ratios. Atmospheric Measurement
866 Technique, 8, 2371-2395, 2015.

867

868 Peters, E., Wittrock, F., GroBmann, K., FrieB, U., Richter, A.,
869 Burrows, J.: Formaldehyde and nitrogen dioxide over the remote western
870 Pacific Ocean: SCIAMACHY and GOME-2 validation using ship-based MAX-
871 DOAS observations. Atmospheric Chemistry and Physics. 12 (22), 11179,
872 2012.

873

874 Picornell, M., Ruiz, T., Borge, R. et al. Population dynamics based
875 on mobile phone data to improve air pollution exposure assessments. J
876 Expo Sci Environ Epidemiol 29, 278-291.
877 <https://doi.org/10.1038/s41370-018-0058-5>, 2019.

878

879 Plane, J.M.C., Saiz-Lopez, A.: UV-Visible Differential Optical
880 Absorption Spectroscopy (DOAS). In: Heard, D.E. (Ed.), Analytical
881 Techniques for Atmospheric Measurement. Blackwell Publishing, Oxford,
882 2006.

883

884 Platt, U., Stutz, J.: Differential Optical Absorption Spectroscopy:
885 Principles and Applications. Springer Berlin Heidelberg, Berlin,
886 Heidelberg, Berlin, Heidelberg, 2008.

887

888 Quaassdorff C, Borge R, Pérez J, Lumbreras J, de la Paz D, de Andrés
889 JM. Microscale traffic simulation and emission estimation in a heavily
890 trafficked roundabout in Madrid (Spain). *Sci Total Environ*, 566-
891 567:416-427. doi:10.1016/j.scitotenv.2016.05.051, 2016.

892

893 Rodgers, C.D.: Inverse Methods for Atmospheric Sounding: Theory and
894 Practice. World Scientific Publishing, Singapore (Singapore), 2000.

895

896 Rothman, L.S., Gordon, I.E., Barber, R.J., Dothe, H., Gamache, R.R.,
897 Goldman, A., Perevalov, V.L., Tashkun, S.A., Tennyson, J.: HITEMP, the
898 high-temperature molecular spectroscopic database *Journal of*
899 *Quantitative Spectroscopy and Radiative Transfer*. 111 (15), 2139,
900 2150, 2010.

901

902 Ryan, R. G., Rhodes, S., Tully, M., Wilson, S., Jones, N., Frieß, U.,
903 and Schofield, R.: Daytime HONO, NO₂ and aerosol distributions from
904 MAX-DOAS observations in Melbourne, *Atmos. Chem. Phys.*, 18, 13969-
905 13985, 2018.

906

907 Saiz-Lopez, A., Borge, R., Notario, A. et al.: Unexpected increase in
908 the oxidation capacity of the urban atmosphere of Madrid, Spain. *Sci*
909 *Rep* 7, 45956. <https://doi.org/10.1038/srep45956>, 2017.

910

911 Schreier, S. F., Richter, A., Peters, E., Ostendorf, M., Schmalwieser,
912 A. W., Weihs, P., & Burrows, J. P: Dual ground-based MAX-DOAS

913 observations in Vienna, Austria: Evaluation of horizontal and temporal
914 NO₂, HCHO, and CHOCHO distributions and comparison with independent
915 data sets. Atmospheric Environment: X 5, 2020

916

917 Serdyunchenko, A., Gorshelev, V., Weber, M., Chehade, W., Burrows,
918 J.P.: High spectral resolution ozone absorption cross-sections - Part
919 2: temperature dependence. Atmospheric Measurement Techniques. 7 (2),
920 625-636, 2014.

921

922 Solomon, S., & Sanders, Ryan W and Schmeltekopf, A. L.: On the
923 Interpretation of Zenith Sky Absorption Measurements. Journal of
924 Geophysical Research, 92, 8311-8319, 1987.

925

926 Stutz, J., Kim, E.S., Platt, U., Bruno, P., Perrino, C., Febo, A.: UV-
927 visible absorption cross sections of nitrous acid. Journal of
928 Geophysical Research: Atmosphere. 105, 14585-14592, 2000.

929

930 Thalman, R., Volkamer, R.: Temperature dependent absorption cross-
931 sections of O₂-O₂ collision pairs between 340 and 630 nm and at
932 atmospherically relevant pressure. Physical Chemistry Chemical Physics
933 15 (37), 15371-15381, 2013.

934

935 Vandaele, A.C., Hermans, C., Simon, P.C., Carleer, M., Colin, R.,
936 Fally, S., Mérienne, M.F., Jenouvrier, A., Coquart, B.: Measurements
937 of the NO₂ absorption cross-section from 42000 cm⁻¹ to 10000 cm⁻²
938 (238-1000 nm) at 220 K and 294 K. Journal of Quantitative Spectroscopy
939 and Radiative Transfer; Atmospheric Spectroscopy Application 59 (3),
940 171-184 96, 1998.

941

942 Wagner, T., Beirle, S., Benavent, N., Bösch, T., Chan, K. L., Donner,
943 S., Dörner, S., Fayt, C., Frieß, U., García-Nieto, D., Gielen, C.,
944 González-Bartolome, D., Gomez, L., Hendrick, F., Henzing, B., Jin, J.
945 L., Lampel, J., Ma, J., Mies, K., Navarro, M., Peters, E., Pinardi,
946 G., Puentedura, O., Puçite, J., Remmers, J., Richter, A., Saiz-Lopez,
947 A., Shaiganfar, R., Sihler, H., Van Roozendaal, M., Wang, Y., and
948 Yela, M.: Is a scaling factor required to obtain closure between
949 measured and modelled atmospheric O₄ absorptions? An assessment of
950 uncertainties of measurements and radiative transfer simulations for
951 2 selected days during the MAD-CAT campaign. *Atmospheric Measurement*
952 *Techniques* 12, 2745–2817, 2019.

953

954 Schreier, S. F., Richter, A., & Burrows, J. P.: Near-surface and path-
955 averaged mixing ratios of NO₂ derived from car DOAS zenith-sky and
956 tower DOAS off-axis measurements in Vienna: A case study. *Atmospheric*
957 *Chemistry and Physics*, 2019.

958

959 Wang, S., Cuevas, C.A., Frieß, U., Saiz-Lopez, A.: MAX-DOAS retrieval
960 of aerosol extinction properties in Madrid, Spain. *Atmospheric*
961 *Measurement Techniques* 9, 5089–5101, 2016.

962

963 Volkamer, R., Spietz, P., Burrows, J., Platt, U.: High-resolution
964 absorption cross-section of glyoxal in the UV-vis and IR spectral
965 ranges. *J. Photochem. Photobiol. Chem.* 172 (1), 35–46, 2005.

966

967 World Health Statistics (WHO): monitoring health for the SDGs. World
968 Health Organization, 2019.

969

970 Yang, T., Si, F., Luo, Y., Zhan, K., Wang, P., Zhou, H., Zhao, M., &
971 Liu, W.:Source contribution analysis of tropospheric NO₂ based on two-
972 dimensional MAX-DOAS measurements. Atmospheric Environment, 2019.